Applied Catalysis B: Environmental 168-169 (2015) 509–514

Contents lists available at ScienceDirect

Applied Catalysis B: Environmental

journal homepage: www.elsevier.com/locate/apcatb

Insights into the twofold role of Cs doping on deN_2O activity of cobalt spinel catalyst—towards rational optimization of the precursor and loading

Gabriela Grzybek*, Paweł Stelmachowski, Sylwia Gudyka, Joanna Duch, Katarzyna Ćmil, Andrzej Kotarba, Zbigniew Sojka

Jagiellonian University, Faculty of Chemistry, Ingardena 3, 30-060 Kraków, Poland

ARTICLE INFO

Article history:
Received 30 October 2014
Received in revised form
31 December 2014
Accepted 9 January 2015
Available online 12 January 2015

Keywords:
Cobalt spinel
Co_3O_4
Alkali doping
Cesium
N_2O decomposition
Mechanistic steps
Surface oxygen species
Work function

ABSTRACT

Cobalt spinel catalysts promoted with different cesium loadings from various precursors (Cs_2CO_3, $CsNO_3$, CH_3COOCs, and CsOH) were prepared by incipient wetness impregnation. The catalysts were characterized by XRF, XRD, SEM, XPS and Raman Spectroscopy. The work function studies were used to optimized the surface doping and monitor the retention of surface oxygen. The stability of cesium promoter was evaluated by means of species resolved – thermal alkali desorption method. The catalytic activity of N_2O decomposition over the synthesized catalysts was studied by temperature programmed reaction. The role of cesium precursor was evaluated in terms of dispersion and the nature of the counterion. The results show that the most active deN_2O catalysts are obtained for cesium carbonate at the narrow loading range of 2–3 atoms/nm^2 (complete N_2O conversion at $T < 200\,^{\circ}C$). The twofold promotional effect is discussed in terms of modification of the electronic properties of the spinel catalyst (stimulation of dissociation step: $N_2O + e = N_2 + O^-$) and stability of the surface oxygen species (recombination step: $O^- = \frac{1}{2}O_2 + e$).

1. Introduction

Nitrous oxide is emitted both from natural nitrogen cycles, and anthropogenic sources, mainly from nitric and adipic acid production. It contributes to the greenhouse effect, and initiates a chain of reactions leading to destruction of the ozone layer [1]. The removal of N_2O from nitric acid plant is still a technological challenge due to severe conditions in the ammonia burner for the high temperature option and for the end-pipe application by a low temperature of the tail gases [2]. Some of the most promising systems for catalytic N_2O removal are based on modified cobalt spinel [3,4]. Improvement of the cobalt spinel catalytic performance may be achieved through a bulk modification by doping with alien cations [5–7], adding various oxides in separate phases [8–10] or by changing the surface properties of the catalyst with alkali promoters [11–13]. The addition of alkali results in a substantial lowering of the reaction temperature window, making such catalytic system potentially suitable for the low temperature applications [14]. This effect has been reported to be mainly of an electronic origin, and associated with the surface promotion, and does not include previously proposed incorporation of alkali ions into the catalyst bulk [1,3]. Presence of the alkali promoters on the catalyst surface lowers the work function of the cobalt spinel facilitating redox processes that occur between the catalyst surface and N_2O reactant. The beneficial influence of the different alkali promoters on the Co_3O_4 activity in nitrous oxide decomposition increases in the order: $Li \ll Na < K < Cs$ [3].

The favorable effect of cesium doping on deN_2O activity was also observed for nickel and copper oxides, and tentatively explained, basing on TPR and XPS results in terms of weakening the metal—oxygen bond, brought about by the modification of electronic state of the transition metal [15,16], leading to higher deN_2O activity.

In our previous studies on deN_2O reaction over Co_3O_4, using isotopically labeled $^{15}N_2{}^{18}O$ molecule, the alkali doping was found to influence recombination of the surface ^{18}O intermediates produced upon the nitrous oxide dissociation [3]:

$$N_2O_{(g)} + e = N_{2(g)} + O_{surf.}{}^- \text{(dissociationstep)}$$

* Corresponding author. Tel.: +48 12 6632017; fax: +48 12 6340515.
E-mail address: maniak@chemia.uj.edu.pl (G. Grzybek).

http://dx.doi.org/10.1016/j.apcatb.2015.01.005
0926-3373/

$O_{surf.}^{-} = \frac{1}{2}O_{2(g)} + e(recombinationstep)$

Changes in the catalytic activity have been directly correlated with the catalyst work function variation upon alkali loading, according to the surface dipole model of Topping [1]. The low work function values promote N_2O dissociation (the first step) by interfacial electron transfer (see above). Although cesium has been shown to exhibit the highest promotional impact on the N_2O turnover, to our best knowledge, there are no systematic studies on the mechanistic role of cesium, its surface loading, precursor nature, and thermal stability at reaction conditions.

In this paper the promotional effect of cesium on the N_2O decomposition over Co_3O_4 catalyst was investigated in detail for a series of cesium several precursors and various loadings. The electronic character of the promotion and the thermal stability of cesium promoter were addressed by means of work function measurement by Kelvin probe and species resolved – thermal alkali desorption methods. The aim of this study was to reveal the comprehensive effect of cesium and its counterion on the deN_2O activity, and provide rational bases for selection of the best precursor and optimize the doping level.

2. Experimental

2.1. Catalyst preparation

The Cs–Co_3O_4 samples were prepared by incipient wetness impregnation of commercially available Co_3O_4 (Fluka) with the use of a water solution of four cesium precursors: Cs_2CO_3, CsOH, $CsNO_3$ and CH_3COOCs. Using appropriate solutions concentrations, a nominal surface loading of cesium in the range of 1–10 atoms/nm^2 was obtained. In the case of carbonate precursor, the samples with the Cs loading of 47 and 94 atoms/nm^2 were also prepared. In the next step, the samples were dried at 100 °C for 2 h, and calcinated in the air atmosphere at 400 °C for 4 h. The number of cesium atoms per nm^2 of cobalt spinel (n_{Cs}) was calculated according to the following equation:

$$n_{Cs} = \frac{x \times c \times V \times N_A}{10^{18} \times S_{BET} \times m_{Co_3O_4}} \quad (1)$$

where x is the number of Cs atoms in cesium precursor molecule, c is the cesium precursor solution concentration [mol dm^{-3}], V is the volume of cesium precursor solution added during Co_3O_4 impregnation [dm^3], N_A is Avogadro number [mol^{-1}], S_{BET} is surface area of cobalt spinel: 16 m^2 g^{-1}, $m_{Co_3O_4}$ is the mass of the impregnated cobalt spinel [g].

2.2. Catalyst characterization

The content of the cesium promoter was determined using an energy-dispersive XRF spectrometer (Thermo Scientific, ARL QUANT'X with the Rh anode, the X-rays of 4–50 kV (1 kV step), 1 mm size beam). A 3.5 mm Si(Li) drifted crystal with a Peltier cooling (~185 K) was used as a detector. The calibration with a series of metallic standards and an UniQuant software were used for quantitative analysis of the results. The XRD measurements were carried out by Bruker D8-advance diffractometer, using CuKα radiation (λ = 1.540598 Å), in the range of 2θ between 10° and 80° with a step of 0.02°. The Raman spectra were recorded at room temperature (Renishaw InVia spectrometer, confocal microscope Leica DMLM, CCD detector with a wavelength excitation of 785 nm). The Raman scattered radiation was registered in the range of 100–800 cm^{-1} with 1 cm^{-1} resolution. In order to provide a sufficient signal to noise ratio, nine scans for each sample were accumulated.

The X-ray photoelectron spectra (XPS) of the Cs-doped catalyst samples were measured with a Prevac photoelectron spectrometer equipped with a hemispherical VG SCIENTA R3000 analyzer. The photoelectron spectra were measured using a monochromatized aluminum AlKα source (E = 1486.6 eV). The base pressure in the analysis chamber during the measurements was 5×10^{-9} mbar. Spectra were recorded with constant pass energy of 100 eV for the survey and narrow scan spectra.

2.3. N_2O decomposition tests

The activity tests of deN_2O reaction for all catalysts were carried out by means of temperature programmed catalytic reaction (TPCR) in a quartz flow reactor, using a 30 mg of sieve fraction of the catalyst (0.2–0.3 mm). The reaction was performed in the atmospheric pressure for a gas mixture (5% N_2O in He) and a total gas flow of 30 ml/min (GHSV = 7000 h^{-1}). The gas composition was monitored by a quadrupole mass spectrometer (RGA200, SRS, lines m/z = 44 (N_2O), 32 (O_2), 30 (NO), 28 (N_2), 18 (H_2O)). The main m/z signals originating from N_2O in QMS are: 44 (62%), 30 (19%), 14 (8%), 28 (7%) and 16 (3%). We have recorded m/z = 30 line to monitor possible formation of NO on the catalyst surface, but since the NO line follows exactly the N_2O profile this possibility can be safely excluded.

To ensure that the reactor is operating in the kinetic regime, the criterial numbers for extra- and intra-granular diffusion limitations were checked according to the EUROKIN procedure [17]. The key input and output parameters are summarized in the Supplementary data (Appendix A).

2.4. Work function measurements

The contact potential difference (V_{CPD}) measurements were carried out by the dynamic condenser method of Kelvin with a KP6500 probe (McAllister Technical Services), which was installed in a vacuum chamber and the catalyst sample was mounted on a heated micrometric manipulator holder. The reference electrode was a standard stainless steel plate with diameter of 3 mm ($WF_{ref} \approx 4.1$ eV) provided by the manufacturer. During the measurements the gradient of the peak-to-peak versus backing potential was set to 0.1, whereas the vibration frequency and the amplitude were set to 120 Hz and 40 a.u., respectively. A single V_{CPD} value was obtained using five backing potentials, each being an average of 32 independent measurements. The final V_{CPD} value was an average of 70 independent points. The work function values were obtained from a simple relation: $eV_{CPD} = WF_{ref} - WF_{sample}$. The work function changes in the presence of O_2 were monitored at 250 °C and 450 °C at the background of 1.0×10^{-6}, and the oxygen pressure of 3.5×10^{-5} and 8.0×10^{-5} mbar. At each conditions the equilibrium signal was reached after 15 min.

2.5. Cesium thermal desorption

The stability of cesium was investigated by the species resolved – thermal alkali desorption (SR–TAD) method [18]. Five samples were selected for the desorption experiments: 2, 2.5, 4, 47 and 94Cs atoms/nm^2 obtained from the Co_3O_4 impregnation with cesium carbonate. The samples in the form of self-supported wafers were placed in the vacuum chamber (10^{-7} mbar), heated from room temperature to 600 °C with temperature steps of 20 °C. Desorption flux of cesium atoms, S/pA, was determined by means of a surface ionization detector [19]. During the measurements, the samples were biased with a positive potential +5 V. In all of the measurements, the resultant positive current was measured directly with a digital electrometer (Keithley 6512), and averaged over 10 independent data points for each temperature. The activation energy (E_{des}) for cesium desorption was calculated with an assumption that the process follows first order kinetics by applying Arrhenius equation justified elsewhere [20,21]. A standard error of

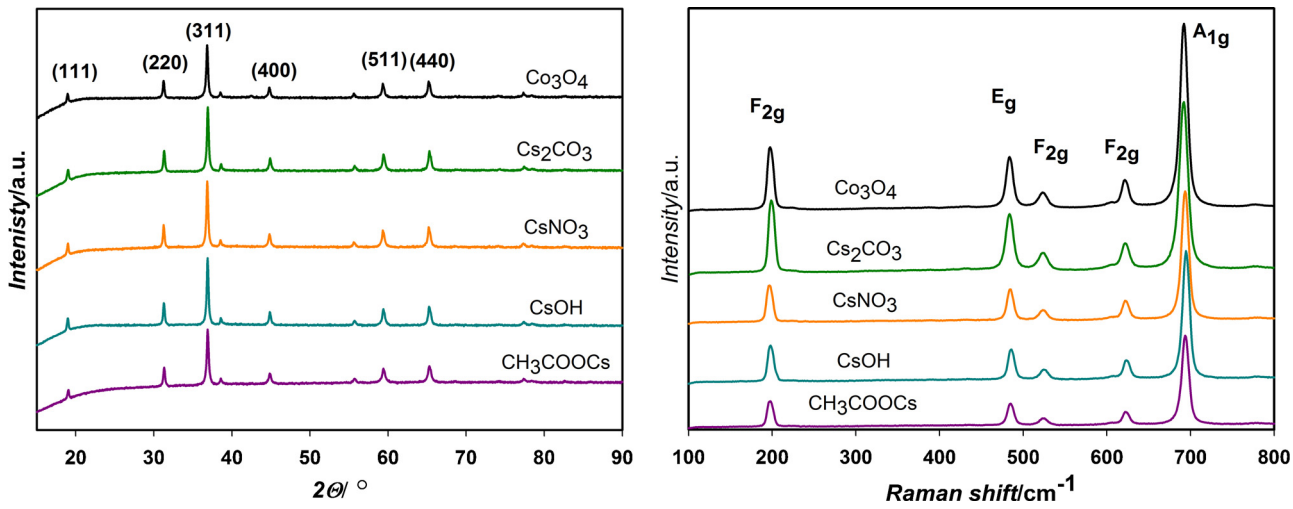

Fig. 1. XRD patterns (a) and Raman spectra (b) of Cs–Co_3O_4 (n_{Cs} = 2.5Cs atoms/nm^2) samples impregnated with different precursors.

the slope from the linear least squares fitting procedure was taken as an error of the E_{des} value.

3. Results and discussion

3.1. Catalyst characterization

The chemical composition of all Cs–Co_3O_4 catalysts determined by XRF measurements is shown in Table 1. The catalysts phase composition was verified by X-ray diffraction and Raman Spectroscopy measurements. All diffractograms of the parent spinel and the Cs-promoted catalysts with the nominal cesium loading of 2.5 atoms/nm^2 are shown in Fig. 1a. The diffraction lines, indexed using ICSD base (69,378-ICSD), at 2θ values of 36.8°, 44.8° and 65.5° related to (3 1 1), (4 0 0) and (4 4 0) planes of Co_3O_4, manifest the presence of cobalt spinel only for all the investigated catalysts. The XRD analysis was supported by Raman spectroscopy (Fig. 1b). Raman peaks located at 196 (F_{2g}), 482 (E_g), 522 (F_{2g}), 619 (F_{2g}) and 691 cm^{-1} (A_{1g}), observed in all spectra confirmed that, as in our previous paper, cobalt is present as Co_3O_4 only [14,22]. Apparently, introducing cesium atoms onto the spinel surface does not lead to appearance of any spurious minor phases such as $CsCoO_2$ [23], that might be undetectable by the XRD due to too small amount. These results are not surprising when the conditions of $CsCoO_2$ formation are taken into account.

The SEM studies of Cs-doped cobalt spinel catalysts obtained with different Cs precursors showed that the micrometric aggregates of the spinel are composed of the crystallites in the size range of 50–150 nm. The cesium doping does not influence the morphology of Co_3O_4 catalyst in an appreciable way. This suggests that the distribution of the promoter is restricted to the surface, as confirmed by spectroscopic studies.

Four cesium carbonate samples were selected for the XPS analysis: 1, 2.5, 5 and 47Cs atom/nm^2 (corresponding to 0.4, 0.9, 1.7 and 13.7 wt%), together with two samples obtained from cesium nitrate (5Cs atoms/nm^2) and acetate (4Cs atoms/nm^2). The analysis of the XPS spectra reveals the presence of all expected component lines: C 1s, O 1s, Cs 3d and Co 2p, for which the peak positions do not differ in an appreciable way for all the investigated samples. In the C 1s energy range two separate peaks were observed, at 285.0 eV and 288.5 eV. The first one was assigned to the adventitious carbon, while the latter can be attributed to carbonate species [24]. Accordingly, the O 1s asymmetric maximum can be decomposed into two peaks, at ca. 530 eV and 531 eV. The relative positions and shape of the Co 2p doublet remain similar regardless the cesium loading (Fig. 2). This indicates that interaction of Cs with spinel does not influence the chemical state of cobalt in an appreciable way. The changes in the Cs 3d peak intensity (Fig. 2) were used for evaluation of the surface atomic concentration of the promoter with

Table 1
The content of cesium (Cs atoms/nm^2) in the doped catalysts series impregnated with different precursors measured by XRF method.

Nominal concentration	Cs precursor			
	Cs_2CO_3	CsOH	$CsNO_3$	CH_3COOCs
1	1.1	1.0	1.1	1.4
2	2.3	1.5	1.9	2.1
2.5	2.6	1.8	2.4	2.7
3	3.4	3.5	3.2	–
4	4.6	3.6	3.6	4.2
5	5.4	5.3	5.6	–
8	8.4	8.3	8.6	8.5
47	61	–	–	–
94	93	–	–	–

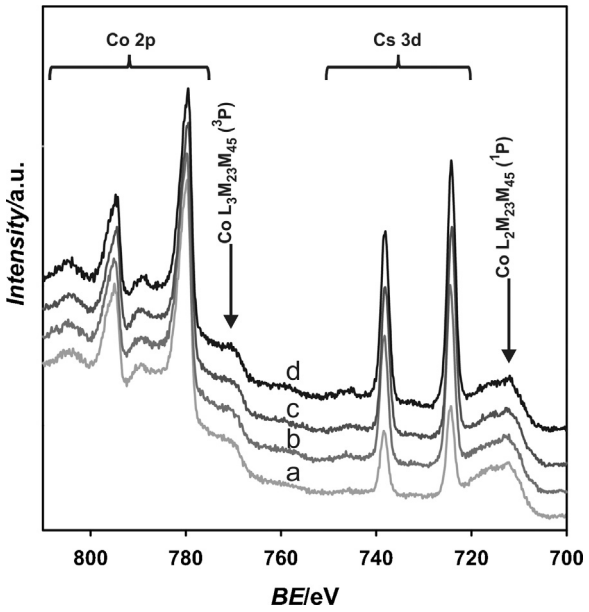

Fig. 2. XPS spectra of the Co 2p and Cs 3d binding energy range for cesium carbonate derived samples.

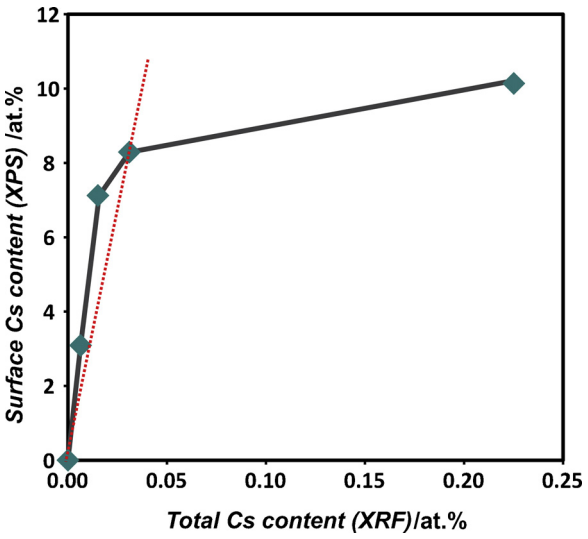

Fig. 3. XPS surface cesium content against XRF cesium loading for carbonate derived samples.

the increasing loading. For the low cesium loadings, the amount of surface cesium (determined from XPS) increases in a linear way with its total amount (determined from XRF). As shown in Fig. 3, surface Cs concentration, after initial linear increase with the loading, stabilizes at the level of ~10 at% (XPS). This reveals that below 5Cs atoms/nm^2 (0.05 at%, XRF) the cesium promoter is well dispersed on the spinel surface, whereas at higher loadings it exhibits tendency for agglomeration. The latter leads to an important lowering of the cesium XPS signal, in comparison with that expected from the extrapolation of the linear region. Analysis of the C 1s signal shows that for the low Cs loadings it is dominated by the carbonate component (288.5 eV), with the Cs/C(carbonate) ratio around the stoichiometric one. However, for higher Cs loadings this ratio increases revealing that in the agglomerated form the carbonate groups are partially decomposed. For other cesium precursors such as $CsNO_3$ and CH_3COOCs a rather weak intensity of the corresponding XPS signals due to the N 1s (407 eV) and C 1s (285.0 and 288.5 eV) revealed that the Cs is predominantly present in an oxide form on the spinel surface. Such results are in agreement with the conclusion that the observed highest promotional effect of Cs_2CO_3 can be associated with the presence of well dispersed cesium in the carbonate form (see below).

3.2. Catalytic N_2O decomposition tests

The temperature programmed catalytic tests were performed for all obtained Cs–Co_3O_4 samples. Basing on these results, the optimal cesium surface concentration over cobalt spinel, for each precursor, was found to be in a narrow range of 2–3Cs atoms/nm^2. In our previous studies we have found that the minimum of the work function corresponds to the highest catalyst activity and the optimum alkali loading appears in a narrow and specific surface coverage [1]. Therefore, the doping level of cesium was optimized with respect to both the catalytic activity and work function value. As an example, typical response profiles for these two parameters ($T_{50\%}$, WF) as a function of the loading are shown in Fig. 4 for cesium carbonate. As can be inferred from Fig. 4 the optimum loading probed by $T_{50\%}$ and WF appears at 2–3Cs atoms/nm^2. Similar behavior was observed for the other precursors with the optimal loading again at the same range but with weaker depths of the $T_{50\%}$ and WF minima.

The comparison of N_2O conversion curves for the optimized catalysts obtained for a particular Cs precursor, presented in Fig. 5,

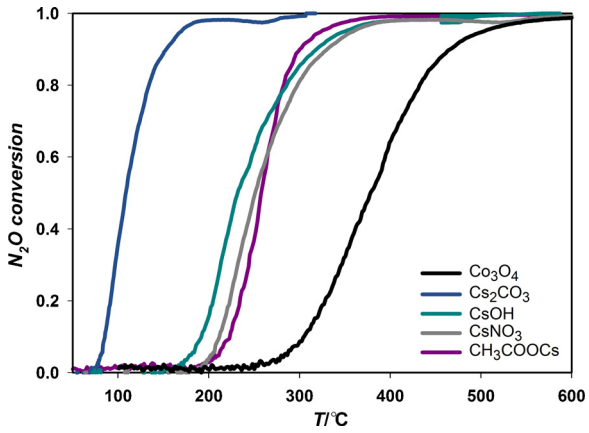

Fig. 4. The conversion curves for N_2O decomposition reaction (TPCR) over the Cs–Co_3O_4 catalysts with cesium loading at 2.5Cs atoms/nm^2.

reveals strong cesium promotional effect, manifested by the shift of the conversion curves to lower temperature by $\Delta T = 250\,^{\circ}C$. Whereas for cesium hydroxide, acetate and nitrite the temperature shift is quite similar (about 130 °C), in the case of carbonate precursor the reaction temperature of 50% conversion ($T_{50\%}$) is further lowered by 100 °C.

The variations of $T_{50\%}$ upon cesium doping at the optimal level (2–3Cs atoms/nm^2) from various precursors is summarized in Fig. 6 with the reference line for the optimized promotional effect of potassium carbonate. Additionally, to assure the absence of diffusion limitation we have also analyzed the changes in the deN_2O activity at lower (10%) conversion ($T_{10\%}$, dark green bars), which provide a consistent picture of the catalyst comparison with that of $T_{50\%}$. This comparison reveals clearly the advantage of replacing potassium by cesium for the effective promotion of cobalt spinel deN_2O catalytic performance, since the latter outperforms potassium by 100 °C (see solid line in Fig. 6).

Noting the low optimal doping level of the alkali promoter 2–3Cs atoms/nm^2 (i.e., ~1 wt%) such replacement should not enhance the catalyst manufacturing cost in an appreciable way despite the pronounce difference in the price of the both alkali metals. These results thus show also that among the investigated counterions CO_3^{2-} exhibits a particularly beneficial role in promoting the deN_2O reaction, therefore, Cs_2CO_3 was selected as the most effective cesium precursor for further investigations.

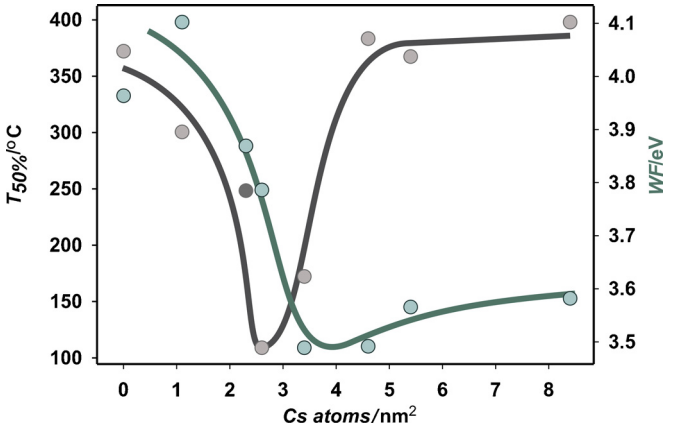

Fig. 5. The work function and half conversion temperature changes as a function of cesium carbonate loading of the cobalt spinel catalyst.

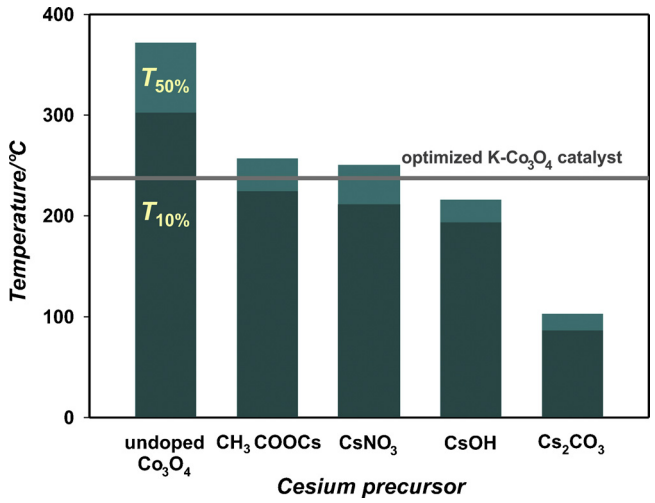

Fig. 6. The comparison of $T_{50\%}$ and $T_{10\%}$ changes upon cesium doping with 2–3Cs atoms/nm^2 from various precursors with the reference line for the optimized potassium carbonate doped Co_3O_4 catalyst. (For interpretation of the references to colour in this figure legend, the reader is referred to the web version of this article.)

3.3. *In situ work function measurements*

As mentioned in Section 1, in the second step of the N_2O decomposition dioxygen is formed via recombination of the surface oxygen intermediates. Therefore, retention of oxygen on the catalyst surface, and the associated effectiveness of the recombination process play a crucial role in closing the catalytic cycle. The Kelvin method was used to probe the interaction of adsorbed oxygen with the catalyst surface via work function changes for bare and optimally Cs-doped Co_3O_4 catalyst (2Cs atoms/nm^2 from carbonate precursor). In Fig. 7 in situ work function results are compared with the reference value measured at the background pressure $p_0 = 10^{-6}$ mbar (before oxygen introduction into the vacuum chamber). The pressure values p_0–p_2 indicate sequential steps of the experiment: reference measurements at the background pressure 1×10^{-6} mbar, oxygen introduction into the chamber at 3.5×10^{-5} mbar and 8.0×10^{-5} mbar; and return to the background pressure.

As shown elsewhere [25], the work function changes are associated with the surface coverage by oxygen species and the extent of their surface ionization. Interaction of *p*-type transition metal oxide with gas phase oxygen leads to appearance of the dinuclear (O_2^- and O_2^{2-}) at 150–250 °C and mononuclear (O^- and O^{2-}) at 350–500 °C surface species. Therefore, the changes in the work function observed in the same temperature range for bare and Cs-promoted Co_3O_4 reflect mainly changes in the oxygen surface coverage at these conditions.

As implied by the data presented in Fig. 7, the changes in the work function upon admission of oxygen are much bigger for bare Co_3O_4 in comparison with the Cs–Co_3O_4 catalyst at 250 °C and decrease at 450 °C. This observation can be interpreted in terms of the higher surface coverage by oxygen for the undoped Co_3O_4 at 250 °C, which approaches the oxygen coverage of Cs–Co_3O_4 at 450 °C. Apparently, the addition of cesium significantly lowers retention of oxygen on the catalyst surface in the temperature range around 250 °C. Additionally, for the Cs-promoted catalyst, in contrast to parent spinel, the work function returns to the initial value, when the oxygen is removed from the gas phase. This indicates reversibility of this surface process and destabilization of surface oxygen upon the Cs promotion. Indeed, comparison of the N_2/O_2 ratio in the temperature range of 200–350 °C reveals appreciable surface retention of oxygen for Co_3O_4 catalyst in contrast to the Cs–Co_3O_4 sample. Taking into account that the N_2O conversion is accomplished below 200 °C such effect of cesium promotion is beneficial for closing the catalytic cycle at such low temperatures. As the oxygen recombination is considered as the rate limiting step of the deN_2O reaction over the cobalt spinel, the observed facilitation of this step is essential for designing the highly active catalyst working at low temperatures.

Following brief discussion in Section 1 the decomposition of N_2O over cobalt spinel can be described in terms of three main steps: activation (NN—O bond cleavage and formation of surface oxygen), diffusion of surface oxygen adatoms and recombination of the latter leading to desorption of dioxygen molecule. Since in all these steps a charge transfer to and from the surface play an important role, they strongly depend on the electronic properties of the catalyst surface, gauged by the work function. Particularly, the first step, where electron transfer from the catalyst surface lead to immediate dissociation of N_2O, strongly depends on the work function of the catalyst. The changes in the work function of the cobalt spinel by cesium doping are presented in Fig. 4. From the combined reactivity and work function measurements it can be concluded that the optimal loading of cesium is in a narrow range of 2–3Cs atoms/nm^2, thus, any small deviations from this value may result in a substantial decrease of the catalytic activity.

3.4. *Cesium thermal desorption*

Promotional effects of alkali dopants are ubiquitously associated with their surface stability [26]. The stability of cesium on the Co_3O_4 surface was assessed from thermal desorption experiments, where a chemical bond between the alkali promoter and the catalyst surface breaks. The desorption parameters (flux and activation energy) evaluated from the SR–TAD experiments provide direct information about the alkali promoter surface stability.

Due to the low work function value of the investigated Cs–Co_3O_4 samples, the main desorption channel of cesium is due to atoms, in agreement with the Saha–Langmuir equation [27]. The appreciable

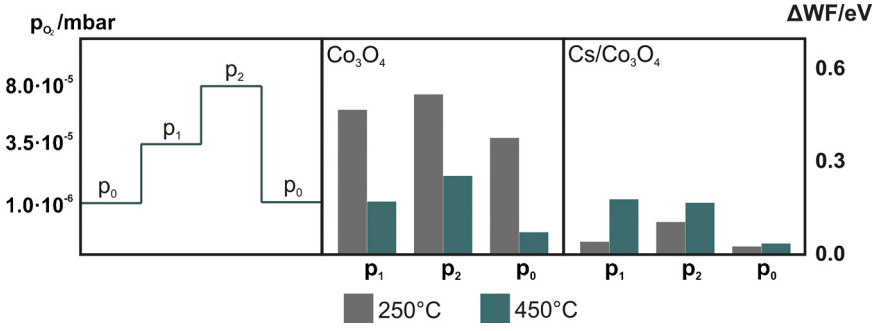

Fig. 7. Changes in the work function for undoped and cesium doped Co_3O_4 (with 2–3Cs atoms/nm^2) upon the variation of oxygen partial pressure at 250 and 450 °C.

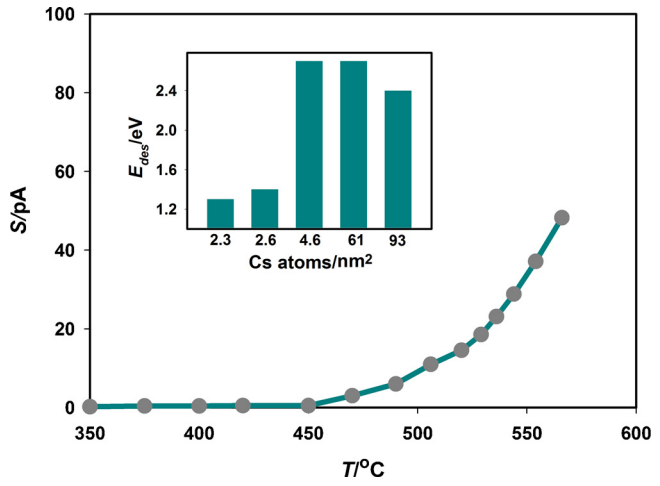

Fig. 8. The desorption signal of cesium as a function of temperature for the optimized Cs–Co_3O_4 catalyst and the desorption barrier for different Cs loadings (insert).

desorption signal starts at $T > 450\,^{\circ}C$, i.e., much above the total N_2O conversion, indicating thus that the promoter is thermally stable in the deN_2O process temperature (Fig. 8). As a result, it can be concluded that the beneficial effect of cesium on cobalt spinel activity shall be preserved in the reaction conditions. The monotonous exponential changes in the cesium signal intensity with temperature indicate that in each case it desorbed from the catalyst surface trough a single barrier. Thus, the corresponding desorption energies were determined from the linear part of the Arrhenius plots (see Fig. 8 insert). The low desorption energies of $E_{des} = 1.3 \pm 0.04$ and 1.4 ± 0.04 eV correspond to the catalysts with the optimal cesium coverage. Such relatively low barriers are characteristic for surfaces with low work function values, confirming the Kelvin probe results. Higher values of E_{des} for higher surface coverages are close to the dissociation energy of the Cs—O bond, which is about 3.0 ± 0.3 eV characteristic for cesium oxide [28]. Thus, for these samples it can be suggested that cesium may be present in the form of Cs_2CO_3/Cs_2O, in-line with partial decomposition of the carbonate revealed by the XPS results. As a result, among the investigated cesium precursors: CsOH, $CsNO_3$, CH_3COOCs, Cs_2CO_3, apart from carbonate all the other precursors turn into Cs_2O to a large extend. Thus, we may expect that their promotional effect on the deN_2O catalytic activity of Co_3O_4 should be similar, as observed indeed in Fig. 5. The CO_3^{2-} counterion, which persists in the reaction conditions shows a distinctly stronger promotional effect. The actual structure of surface cesium carbonate has not been elucidated as yet. Taking into account the changes of the spinel work function we may infer that the surface dispersion and/or formation of the surface $Cs^{\delta+} - O_{surf}^{\delta-}$ dipoles that counterbalance the surface potential barrier for electron transfer are considerably higher for Cs_2CO_3 than for Cs_2O (produced by decomposition of other precursors during the catalyst pretreatment).

Summarizing, although the spinel samples with higher cesium loadings exhibit better thermal stability, the promotional effect is, in this case, definitely lower. Nevertheless, the thermal stability of cesium at the optimal loading is good enough for low temperature applications, yet they exhibit substantially better deN_2O reactivity. Thus, the overloading of the alkali promoter will have no clear practical benefit on the long term catalyst activity.

4. Conclusions

A series of Cs–Co_3O_4 catalysts with different cesium loadings were prepared by incipient wetness impregnation. Among the various precursors studied (Cs_2CO_3, $CsNO_3$, CH_3COOCs, and CsOH) the highest catalytic activity was observed for the cesium carbonate precursor, reaching spectacular 100% conversion of N_2O below $200\,^{\circ}C$. The optimal cesium loading confined to a narrow range of 2–3 atoms/nm^2 was determined based on the work function measurements and activity profiles. As revealed by the desorption experiments the cesium promoter is thermal stabile at the reaction conditions (below $450\,^{\circ}C$). It is shown that the promotional effect is twofold and consist in lowering the work function, which favors the first step of N_2O decomposition, and destabilization of the surface oxygen species, which is beneficial for closing the catalytic cycle.

Acknowledgements

The project was financed by the Polish National Science Center awarded by decision number DEC-2011/03/B/ST5/01564. The research was carried out with the equipment purchased thanks to the financial support of the European Regional Development Fund in the framework of the Polish Innovation Economy Operational Program (contract no. POIG.02.01.00-12-023/08).

Appendix A. Supplementary data

Supplementary data associated with this article can be found, in the online version, at http://dx.doi.org/10.1016/j.apcatb.2015.01.005.

References

[1] F.A. Zasada, P. Stelmachowski, G. Maniak, J.-F. Paul, A. Kotarba, Z. Sojka, Catal. Lett. 127 (2009) 126–131.
[2] J. Perez-Ramirez, F. Kapteijn, K. Schoffel, J.A. Moulijn, Appl. Catal. B 44 (2003) 117.
[3] P. Stelmachowski, G. Maniak, A. Kotarba, Z.J. Sojka, Catal. Commun. 10 (2009) 1062–1065.
[4] K. Karásková, L. Obalová, F. Kovanda, Catal. Today 176 (2011) 208–211.
[5] K. Omata, T. Takada, S. Kasahara, M. Yamada, Appli. Catal. A 146 (1996) 255–267.
[6] L. Yan, T. Ren, X. Wang, D. Ji, J. Suo, Appl. Catal. B 45 (2003) 85–90.
[7] L. Yan, T. Ren, X. Wang, Q. Gao, D. Ji, J. Suo, Catal. Commun. 4 (2003) 505–509.
[8] F. Kovanda, T. Rojka, J. Dobešová, V. Machovič, P. Bezdička, L. Obalová, K. Jirátová, T. Grygar, J. Solid State Chem. 179 (2006) 812–823.
[9] R. Dziembaj, M.M. Zaitz, M. Rutkowska, M. Molenda, L. Chmielarz, Catal. Today 191 (2012) 121–124.
[10] L. Xue, C. Zhang, H. He, Y. Teraoka, Appl. Catal. B 3–4 (2007) 167–174.
[11] H. Yoshino, C.H. Ohnishi, S. Hosokawa, K. Wada, M. Inoue, J. Mater. Sci. 46 (2011) 797–805.
[12] K. Asano, C. Ohnishi, S. Iwamoto, Y. Shioya, M. Inoue, Appl. Catal. B 78 (2008) 242–249.
[13] L. Obalová, K. Karásková, K. Jirátová, F. Kovanda, Appl. Catal. B 90 (2009) 132–140.
[14] G. Maniak, P. Stelmachowski, A. Kotarba, Z. Sojka, V. Rico-Pérez, A. Bueno-López, Appl. Catal. B 136 (2013) 302–307.
[15] N. Pasha, N. Lingaiah, P.S.S. Reddy, P.S.S. Prasad, Catal. Lett. 127 (2009) 101–106.
[16] N. Pasha, N. Lingaiah, P.S.S. Reddy, P.S.S. Prasad, Catal. Lett. 118 (2007) 64–68.
[17] EUROKIN_fixed-bed_html, EUROKIN spreadsheet on requirements for measurement of intrinsic kinetics in the gas-solid fixed-bed reactor, (2012), www.eurokin.org
[18] A. Kotarba, I. Kruk, Z. Sojka, J. Catal. 211 (2002) 265–272.
[19] K. Engvall, L. Holmlid, A. Kotarba, J.B.C. Pettersson, P.G. Menon, P. Skaugset, Appl. Catal. A 134 (1996) 239–246.
[20] A. Kotarba, J. Dmytrzyk, W. Raróg-Pilecka, Z. Kowalczyk, Appl. Surf. Sci. 207 (2003) 327–333.
[21] M. Hagström, K. Engvall, J.B.C. Pettersson, Phys. Chem. B 104 (2000) 4457–4462.
[22] V.G. Hadjiev, M.N. Iliev, I.V.J. Vergilov, J. Phys. C 21 (1988) L199–L201.
[23] N.Z. Ali, J. Nuss, R.K. Kremer, M. Jansen, Inorg. Chem. 51 (2012) 12336–12342.
[24] L.A. Langley, D.E. Villanueva, D.H. Fairbrother, Chem. Mater. 18 (2006) 169–178.
[25] N. Barsan, U. Weimar, J. Electroceram. 7 (2001) 143–167.
[26] W.D. Mross, Cat. Rev. Sci. Eng. 25 (1983) 591–637.
[27] G.A. Samorjai, Introduction to Surface Chemistry and Catalysis, John Wiley & Sons Inc., 1994.
[28] "Bond dissociation energies", in: David Lide, (Ed.), CRC Handbook of Chemistry and Physics, 87th ed., Internet Version, (2007).